

pubs.acs.org/Macromolecules Article

A Hidden Relaxation Process in Poly(2-vinylpyridine) Homopolymers, Copolymers, and Nanocomposites

Walter W. Young, Hiromu Tabuchi, Ryo Iguchi, Takashi Konishi, Koji Fukao,* and Reika Katsumata*



Cite This: *Macromolecules* 2022, 55, 6590–6597



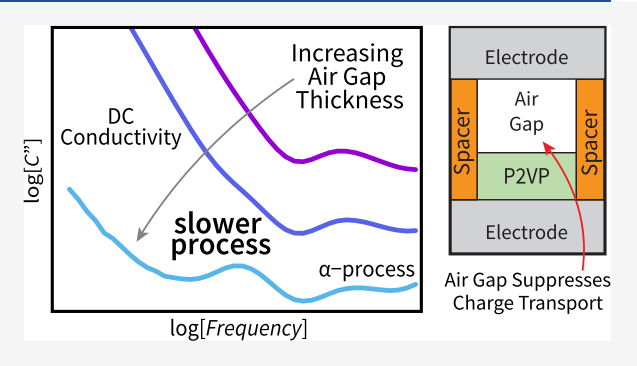
ACCESS I

Metrics & More

Article Recommendations

Supporting Information

ABSTRACT: In broadband dielectric spectroscopy experiments, we find that introducing an air gap between the top electrode and the polymer sample reduces DC conductivity substantially, allowing the study of low-frequency relaxations, whose signal would otherwise be hidden by the DC conductivity signal. An extra process slower than the α -relaxation process is observed in poly(2-vinylpyridine) (P2VP), consistent with some earlier reports. This "slower process" was studied in two heterogeneous systems to examine the interaction between the 2VP and other species to elucidate the mechanism behind the slower process signal. In a random copolymer of styrene and 2VP, the relaxation strength of the slower process relative to the α -process increases substantially at low 2VP mole fractions. Additionally, in a



composite of P2VP and octa(aminophenyl) silses quioxane (OAPS), the presence of OAPS increases both the strength and time scale of the slower process, leaving the α -relaxation process relatively unchanged. This suggests that the slower process could be caused by cooperative polymer relaxation coupled to the transport of heterogeneous components and impurities. Further studies are needed to probe the molecular-level mechanism of this slower process and its effect on interfacial properties.

■ INTRODUCTION

The physical behavior of a polymer material is fundamentally the polymer chains' ability to respond to an applied field as a function of time and length scale. On most experimentally relevant time temperature scales, polymer dynamics are well modeled by the α relaxation process at short times, Rouse dynamics at moderate times, and entanglement relaxations at long times. Dielectric relaxation spectroscopy (DRS) has proven to be an invaluable tool to study these polymer relaxation behaviors by applying an oscillating electric field to an insulating material between two electrode plates acting as a capacitor.2 The rearrangement of polymer molecules generates a capacitance that varies with the frequency of the applied electric field, according to the mobility of the rearranging component. The segmental α -relaxation process in polymers, which is crucial to understanding the glass transition, is a representative example where DRS is the most widespread observation method. In addition to the relaxation processes general to all polymers, system-specific relaxation processes have been observed by DRS and mechanical spectroscopy.³ Some well-studied examples of such anomalous behaviors include methyl group spin in poly(n-alkyl methacrylates)4,5 and relaxations in the deeply supercooled regime in polycarbonate, which contribute to mechanical toughness in the glassy regime. 6-10

One atypical polymer relaxation process that remains poorly understood is the "slower process" in poly(2-vinylpyridine) (P2VP), which appears on timescales longer than the α -relaxation time in DRS measurements, and is of uncertain

dynamic origin.¹¹ Studying the slower process of P2VP is a critical research thrust because a large portion of fundamental studies of nanocomposite dynamics use P2VP as a model polymer matrix, leveraging its ability to form hydrogen bonds with fillers. 12-16 For example, across multiple polymers, including P2VP, observations of dynamic slowdown in nanoparticle-polymer interphases via DRS have distinguished the "bound polymer layer" (polymer extending $\sim 2R_g$ from the nanoparticle surface, which exhibits very slow diffusion but unperturbed segmental relaxation) from the "interfacial layer" (polymer segments extending several nanometers from the nanoparticle surface with severely hindered segmental relaxation kinetics). 17-21 Understanding the relaxation behavior of polymer chains confined by nanoparticles remains a challenge in developing a first-principles model of polymer nanocomposite properties. This is key to building advanced hybrid materials with mechanical, electrical, thermal, and transport properties that are superior to an unmodified polymer material.2

Herein, we use DRS to observe the slower process in P2VP as a function of temperature and frequency in heterogeneous systems

Received: April 17, 2022 Revised: July 5, 2022 Published: July 28, 2022





and assign the origin of the slower process to conformational isotropization (i.e., rotation of the pyridine ring pendant to the polymer backbone) and charge carrier motions on the length scale of monomers. The slower process can be observed clearly by introducing an air gap between the polymer film and the upper electrode, which suppresses DC conductivity. The effect of the local environment on the slower process is first studied in statistical copolymers of styrene and 2-vinylpyridine (2VP). These monomers are similar in their molecular shape and glass transition temperature, with the primary difference being the high polarity of the 2VP monomer compared to styrene. The motion of polar groups such as the pyridine ring in 2VP tends to dominate the dielectric response, so the addition of less polar styrene units was hypothesized to weaken the slower process response. We find that the slower process increases in characteristic timescale as styrene content increases in a copolymer, yet the strength of the slower process remains strong relative to the strength of the α -process across all compositions. Interestingly, the α -relaxation time we measure has a weaker dependence on OAPS loading relative to previous reports. 14,15 This suggests that the mechanism of the slower process may be coupled to the transport of impurities. To test the hypothesis, a model nanocomposite was studied, with the nanofiller, octa-(aminophenyl) silsesquioxane (OAPS), acting as a hypothetical impurity. We observe that the addition of OAPS to the system substantially increases the slow process time, in line with the hypothesis that the slow process is coupled to transport within the polymer matrix.

■ RESULTS AND DISCUSSION

By introducing an air gap between the upper electrode and the model polymer poly(2-vinyl pyridine) (P2VP) film in DRS measurements (Figure 1), we were able to observe slower

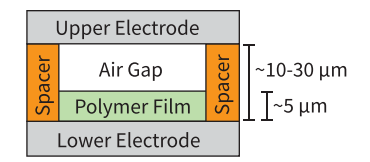


Figure 1. Schematic picture of the sample film of P2VP with a Kapton spacer between two electrodes (side view).

processes that are typically buried underneath the strong signal originating from DC conductivity. $^{11-16}\,\rm DC$ conductivity occurs at low frequencies in DRS measurements of insulating materials such as polymers when charge-carrying impurities have sufficient time to travel between electrodes, resulting in current flow.² This is observed as a characteristic signal with scaling $C'' \approx f^{-1}$, where C'' is the imaginary part of the complex electric capacitance of the dielectric setup and f is the measurement frequency of applied electric field. With an air gap, the DC conductivity is reduced, which allows us to observe relaxation processes in a much lower frequency region compared to previous works. 11-16 In other words, charge carriers present in the sample are partially prevented from moving between electrodes because the air acts as an electrical insulator. Notably, air gaps between the upper electrode and polymer film in DRS measurements have been used to study the free surface of polymer thin films, with minimal contributions from Maxwell-Wagner-Sillars (MWS) polarization due to the relatively low conductivity of the polymer. 23,24

The influence of the air gap thickness on DC conductivity is studied in the model polymer poly(2-vinylpyridine) (P2VP).

The frequency dependence of the imaginary part of the complex electric capacitance C'' at 408 K for \sim 5 μ m P2VP drop-cast films with electrodes separated by Kapton spacers of variable thickness is given in Figure 2. Because the effective area of the electrode is

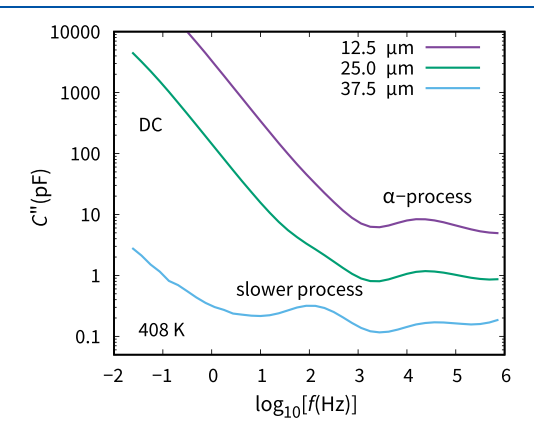


Figure 2. Spacer thickness dependence of the imaginary part of electric capacitance of P2VP thin films at 408 K. At a large spacer thickness (37.5 μ m), the slower process becomes apparent due to the suppression of DC conductivity between electrodes.

kept constant across all measurements, the measured capacitance decreases as increasing spacer thickness, reducing the total measurement signal. When the Kapton spacer is 12.5 μ m thick, there is a dielectric loss peak due to the α -process just above 10⁴ Hz and a large contribution from the DC conductivity below 10³ Hz at 408 K, which is described by the loss component proportional to f^{-1} . At a spacer thickness of 25.0 μ m, a small shoulder appears around 10² Hz. When the thickness of the spacer is 37.5 μ m and the contribution from the DC conductivity is substantially reduced, a clear peak emerges at 10^2 Hz. This peak occurs in addition to the loss peak corresponding to the α process, which remains present in all samples. This extra process around 10² Hz corresponds well to the slower process inferred previously in P2VP, though this was previously only observed in the derivative of the real part of complex dielectric permittivity. 11 The physical origin is possibly caused by the conformational isotropization proposed by Spiess et al. for poly(n-alkylmethacrylates).5

A good agreement between the measured complex capacitance and calculations from an equivalent circuit model indicates that the air gap between the samples and the electrode is responsible for the suppression of the DC conductivity. As the thickness of the Kapton spacer increases, the thickness of the air gap between the upper electrode and the surface of the P2VP film also increases (Figure 1). Assuming a parallel circuit of the condenser of the Kapton spacer and the condenser composed of the air gap and P2VP film in series, the observed total complex electric capacitance C^* can be described by

$$C^* = C_k^* + \frac{C_a C_s^*}{C_a + C_s^*} \tag{1}$$

where C_k^* , C_a , and C_s^* are the electric capacitances of the Kapton spacer, the air gap, and the P2VP film, respectively. The three capacitances are given by

$$C_{k}^{*} = \varepsilon_{0} \varepsilon_{k}^{*} \frac{S_{k}}{d_{k}}, C_{a} = \varepsilon_{0} \frac{S_{a}}{d_{k} - d_{s}}, C_{s}^{*} = \varepsilon_{0} \varepsilon_{s}^{*} \frac{S_{a}}{d_{s}}$$
(2)

where ε_0 is the permittivity of the vacuum, ε_k^* and ε_s^* are the complex permittivities of the Kapton and the P2VP, S_k and S_a are the areas of the Kapton spacer and the air gap layer, and d_k and d_s are the thicknesses of the Kapton spacer and the P2VP film, respectively. If the imaginary part of the dielectric permittivity is much smaller than the real part of the dielectric permittivity, the imaginary part of the total electric capacitance C'' is approximately given by

$$C'' \approx \left(\frac{C_{\rm a}}{C_{\rm a} + C_{\rm s}'}\right)^2 \times C_{\rm s}'' + C_{\rm k}'' \tag{3}$$

where $C_{\rm s}{'}$ and $C_{\rm s}{''}$ are the real and imaginary parts of the complex electric capacitance of the P2VP film, and $C_{\rm k}{''}$ is the imaginary part of the complex electric capacitance of the Kapton spacer. The values of the imaginary part of the complex electric capacitance at the peak frequency of the α -process at 408 K are shown in Table 1, obtained using eq 3. The dielectric permittivity of P2VP is

Table 1. Imaginary Part of the Complex Electric Capacitance at the Peak Frequency of the α -Process at 408 K: Measured Versus Calculated

$d_{k}\left(\mu \mathbf{m}\right)$	$C''_{\alpha, \text{ max}}$ (pF) (calculated)	$C''_{\alpha, \text{ max}}$ (pF) (observed)
12.5	8.2	8.3
25.0	1.4	1.2
37.5	0.5	0.2

taken to be $\varepsilon_s'\approx 4$ and $\varepsilon_s''\approx 1$ at the α -peak position. ^{11,25} Though the thicknesses of real films were not completely uniform, the effective thickness of the P2VP thin film is approximated to be 5 μ m, which is used to convert the measured capacitance to dielectric permittivity using eq 2. These values are compared to the values found experimentally in Figure 2. The reasonable agreement between calculated and observed values as a function of spacer thickness (Table 1) validates our equivalent circuit model to explain the influences of the air gap. The existence of the air gap between the upper electrode and the surface of the P2VP thin film can suppress DC conductivity in the imaginary part of the electric capacitance, revealing the hidden extra relaxation process. Hereafter, ε_s'' evaluated by eqs 2 and 3 is denoted as ε'' .

To further understand the possible mechanism of the slower process and to determine if it could be related to conformational isotropizations observed previously by Spiess and coworkers,⁵ random copolymers of styrene and 2-vinyl pyridine (P(S-2VP))were synthesized via reversible addition-fragmentation chaintransfer (RAFT) polymerization²⁶ and studied using the air gap method in DRS. The RAFT copolymers of styrene and 2VP can be considered random with no substantial blocks of either monomer or a gradient of monomer composition.²⁶ This was shown previously through the study of the reactivity ratios of the two monomers during polymerization and the 13C NMR spectrum of the resultant copolymer. There was no observable monomer drift during polymerization, and the measured incorporation of 2VP was close to the target value, implying no composition gradient. In the ¹³C NMR spectrum of a P2VP homopolymer, peaks are observed, which correspond to the tacticity of neighboring 2VP monomers, but these peaks were not observed in P(S-2VP), indicating qualitatively a lack of blocky repeat units in the copolymers. In Table 2, the fraction of 2VP, f_{2VP} , the number-averaged molecular weight, M_n , the dispersity of the molecular weight, \mathcal{D} , the glass transition temperature, T_{g} , and the thickness of each sample measured by atomic force

Table 2. Polymer Compositions and Characterizations of P(S-2VP) Copolymers

$f_{2\text{VP}}$	$M_{\rm n}$ (kDa)	$\mathcal D$	$T_{g}(K)^{a}$	$d_{\rm s}\left(\mu{\rm m}\right)$
1.00 ^b	5	1.04	347.1 ± 2.6	6 ± 1
0.82	15	1.10	366.8 ± 1.0	5 ± 1
0.78	15	1.11	369.4 ± 1.0	8 ± 1
0.77	15	1.15	367.5 ± 1.0	4 ± 1
0.71	16	1.08	368.1 ± 0.7	6 ± 1
0.64	10	1.14	365.5 ± 0.4	4 ± 1
0.55	12	1.16	369.6 ± 0.2	6 ± 1
0.27	10	1.10	368.9 ± 0.3	4 ± 1
0.10	13	1.10	362.6 ± 0.9	4 ± 1
0.00	5	1.15	356.1 ± 0.8	4 ± 1

 $^aT_{\rm g}$ determined from dielectric measurements using $au_a(T_{\rm g})=10^2$ s, where au_a is the relaxation time of the lpha-process. b P2VP homopolymer is purchased from Polymer Source, Co., Ltd.

microscopy (AFM) and capacitance measurements are listed for P(S-2VP) copolymers. The styrene comonomer was chosen because it is known to have a similar $T_{\rm g}$ and molar volume as P2VP while having a far weaker dielectric response due to its much lower dipole strength. 27,28

Leveraging the choice of comonomers, we hypothesized that the strength of the slower process would decrease according to the fraction of styrene in the copolymer, which could be used to determine an effective length scale over which the slower process stops occurring due to too many non-interacting styrene monomers. Representative dielectric loss data of copolymer as a function of frequency and temperature are shown in Figure 3, with the full data set in Figure S4. Surprisingly, slower processes were observed even for polystyrene homopolymers but at much lower frequencies. This effect persisted for polymers regardless of whether the dithioester RAFT endgroup was cleaved and removed, indicating that there were no significant effects caused by the endgroup or any possible contamination by dithioesters that may have cleaved to form a small molecule during the DRS measurements at high temperatures (Figure S4j,k).

The complete set of copolymers studied is shown in Figure 4a, with their dielectric loss ε'' plotted versus frequency at 403 K. Two clear trends emerge, first, that the timescale of the α -process is mostly independent of $f_{\rm 2VP}$, and second, that the timescale of the slower process increases by approximately 3 orders of magnitude between the P2VP and PS homopolymers. We note that PS homopolymer ($f_{\rm 2VP}=0.00$) and P2VP homopolymer ($f_{\rm 2VP}=1.00$) have lower molecular weight than other copolymers, leading to low $T_{\rm g}$ and higher frequency for α -process. The frequency dependence of ε'' at a given temperature can be well reproduced using the following equation for the complex dielectric permittivity $\varepsilon_{\rm s}^*$ of P(S-2VP) copolymers:

$$\varepsilon_{\rm s}^*(\omega, T) = \varepsilon_{\infty} + \sum_{i=\alpha, {\rm s}} \frac{\Delta \varepsilon_i}{(1 + (i\omega \tau_i)^{\alpha_i})^{\beta_i}} + i \frac{\sigma}{\varepsilon_0 \omega}$$
(4)

where $\omega=2\pi f$, ε_{∞} is the dielectric permittivity at very high frequency, $\Delta\varepsilon_{i}$, τ_{i} , α_{i} , and β_{i} are the dielectric relaxation strength, the relaxation time, the distribution parameter of the relaxation time, and the asymmetry parameter of the *i*-process, respectively (Table S1). Here, *i* corresponds to the α -process or the slower process. The term on the right end is present to account for the presence of DC conductivity at low frequencies, where σ is the steady-state conductivity of the polymer. The relaxation rate $f_{i,\max}$ and the dielectric loss maximum $\varepsilon''_{i,\max}$ of

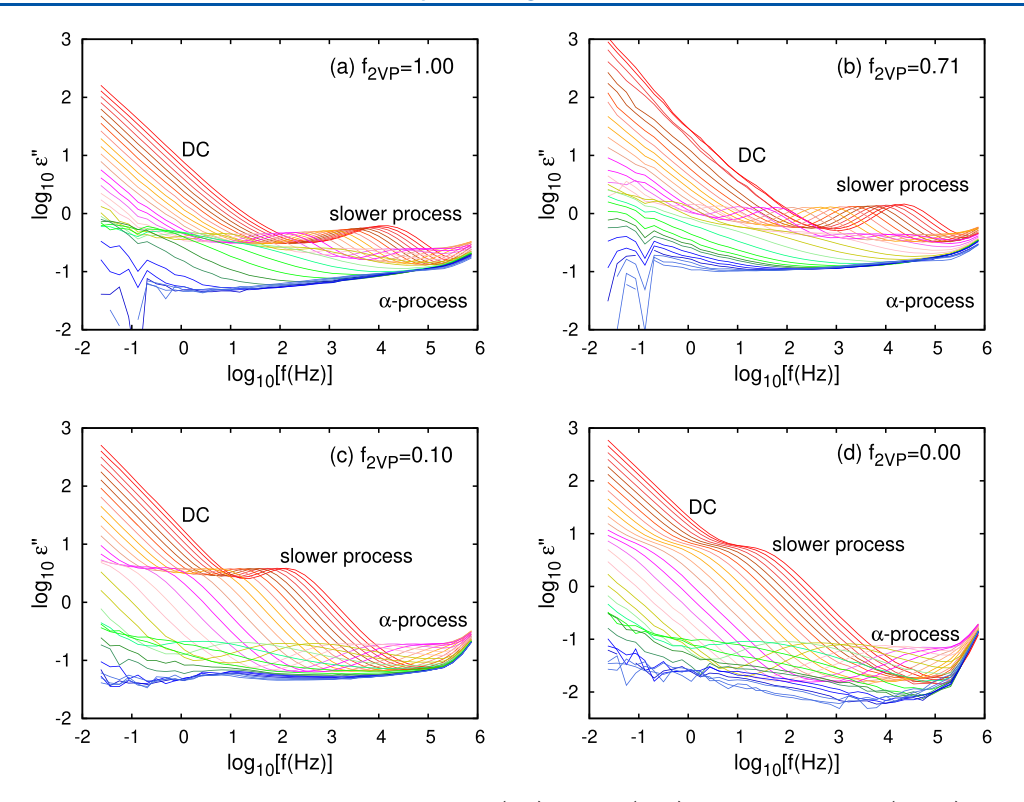


Figure 3. Frequency dependence of ε'' at various temperatures from 473 K (red) to 293 K (blue) at intervals of 5 K for P(S-2VP) copolymers with various fractions of 2VP, $f_{\rm 2VP} = 1.00$ to 0.00. (a) $f_{\rm 2VP} = 1.00$, P2VP homopolymer, (b) $f_{\rm 2VP} = 0.71$, (c) $f_{\rm 2VP} = 0.10$, (d) $f_{\rm 2VP} = 0.00$. Kapton spacer with the thickness of 37.5 μ m was used. The position of the slower process shifts to lower frequency for lower $f_{\rm 2VP}$ polymers.

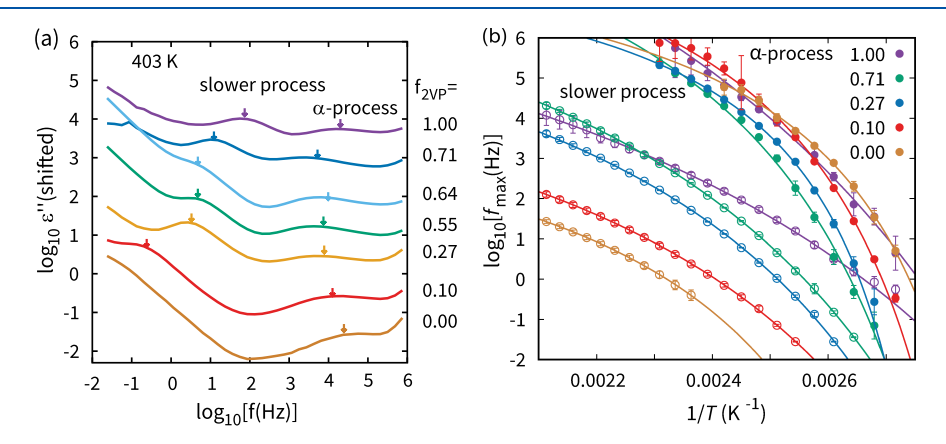


Figure 4. (a) Imaginary part of dielectric permittivity of P(S-2VP) films with variable 2VP content measured with a Kapton spacer thickness of 37.5 μ m. Curves are shifted vertically for clarity. The shift amounts are -0.4, 0.14, 1.15, 1.45, 1.95, 3.35, and 4.20 for $f_{\rm 2VP}$ = 0.00, 0.10, 0.27, 0.55, 0.64, 0.71, and 1.00, respectively. The relaxation time of the α-process is essentially independent of $f_{\rm 2VP}$, while the relaxation time of the slower process decreases substantially with increasing $f_{\rm 2VP}$. (b) Arrhenius plot of the slower process and the α-process, demonstrating the validity of VFT law for each process. Fitting parameters are shown in Table S2.

the i-process can be evaluated from the fitting parameters using the equations

$$f_{i,\text{max}} = \frac{1}{2\pi\tau_i} \left(\frac{\sin\frac{\pi}{2} \frac{\alpha_i}{\beta_i + 1}}{\sin\frac{\pi}{2} \frac{\alpha_i \beta_i}{\beta_i + 1}} \right)^{1/\alpha_i},$$

$$\varepsilon_{i,\text{max}}'' = \Delta \varepsilon_i \frac{\left(\sin\frac{\pi \alpha_i \beta_i}{2(1 + \beta_i)}\right)^{\beta_i + 1}}{\left(\sin\frac{\pi}{2} \alpha_i\right)^{\beta_i}}$$
(5)

In the case of $\beta_i = 1$, the relation $2\pi f_{i, \text{max}} \cdot \tau_i = 1$ holds.

The relaxation rates $f_{i, \text{max}}$ of the slower and α -processes are plotted versus the inverse of temperature in Figure 4b, which shows that the relaxation times of both processes have a Vogel–Fulcher–Tammann (VFT) temperature dependence as follows:

$$\frac{\tau_i(T)}{\tau_{i,0}} = \exp\left(\frac{U_i}{T - T_{i,0}}\right) \tag{6}$$

where $\tau_{i,0}$ and U_i are positive constants, and $T_{i,0}$ is the Vogel temperature for the *i*-process, either the α -process or slower process. This VFT is characteristic of the α -process in polymers but is not well studied for the slower process beyond its initial

discovery by Papadopoulos et al. ¹¹ It is intriguing that the composition dependence of $T_{\rm g}$ and fragility of the α -process and slower process are quite different (Table S2).

By comparing the strength of the slower and the α -relaxation processes, the slower process is shown to contribute significantly to the dielectric response of the polymer even at low $f_{\rm 2VP}$. From dielectric loss spectra, the values of ε'' at the peak frequency of the α - and slower processes are compared for each value of $f_{\rm 2VP}$. Assuming that the width of the loss peaks is the same for the two processes, this corresponds to the relaxation strength due to the slower process relative to that of the α -process. To avoid possible uncertainty induced by the variation in thickness, we adopt the dielectric strength of the slower process relative to the strength of the α -process. This is expressed as the ratio $\frac{\varepsilon''_{n,\max}}{\varepsilon''_{n,\max}}$, shown in Figure

5 as a function of f_{2VP} . The relative relaxation strength of the

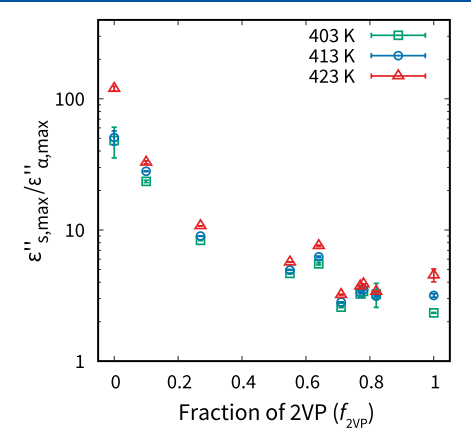


Figure 5. Ratio of the slower process relaxation strength to that of the α -process as a function of 2VP fraction. Relative to the α -process, the slower process is much stronger at low $f_{\rm 2VP}$.

slower process to that of the α -process increases with the decrease of $f_{2\text{VP}}$ and holds across three different temperatures. In particular, the relaxation strength of the slower process for 2VP fractions of $f_{2VP} = 0.00$ and 0.10 is several tens of times as large as that of the α -process. We hypothesize that this trend might be rationalized by the assumption that the slower process is strongly coupled to the movement of charge-carrying groups. Considering that DC conductivity is routinely observed across all polymer materials studied by DRS and requires the presence of mobile charge carriers even at very low amounts,2 it is reasonable to assume that any polymer sample used in a DRS measurement has impurities capable of carrying charge. However, the overall level of charge carriers must be low; otherwise, MWS polarization would be evident due to charge accumulation at the air-polymer interface. An evaluation of the peak position and relaxation strength of dielectric loss peak from a possible MWS process in our study shows that the expected location and strength are different from those observed for the slower process, as detailed in the Supporting Information.

Recently, Song et al. reported slower processes in PS and other polymers above their glass transition temperatures.³⁴ The authors related the slow process to the time scale for spontaneous rearrangements and equilibration in liquids, while the molecular-level mechanism is still unclear. This observation is consistent with Lupaşcu et al.'s former work that also observed slow relaxation processes in PS.³⁵ In this paper, the process was assigned to a helix defect mechanism related to T2G2 helix

conformations. Notably, both relaxation processes can be described by Arrhenius scaling with a reasonable match in time scales, while our result suggests that the temperature dependence is rather VFT-like (Figure S5). We also note that the α -relaxation time between Song et al.'s and ours agree very well, unlike the slower process. The difference in the temperature dependence of the slower process could be associated with uncertainty originating from the separation procedures of the slower process from the DC conductivity contribution above the glass transition temperature. Although further measurements are required to elucidate the physical mechanism of the slower process, such previous works highlight the importance of the slower process to understand a wider range of physical phenomena in polymer thin films.

To further understand the interaction between the slower process of P2VP and chemically distinct fillers, octa-(aminophenyl) silsesquioxane (OAPS) was loaded into P2VP at various weight fractions by solution-casting from tetrahydrofuran and annealing above $T_{\rm g}$ under vacuum for 2 days to create a model nanocomposite. To confirm that the OAPS, which is an amine-functionalized polyoctahedral silsesquioxane (POSS), was well dispersed in the P2VP matrix in the bulk states, X-ray scattering measurements were performed. In addition to the measurements of the bulk, the X-ray measurements on thin films of P2VP and OAPS nanocomposites were performed using the GISAXS (grazing-incidence small-angle X-ray scattering) technique. See in Figure 6, there are no

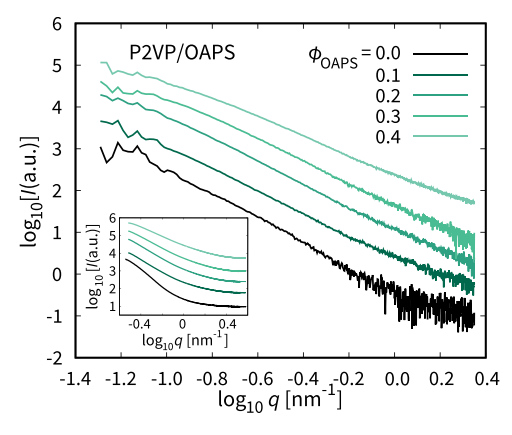


Figure 6. X-ray scattering intensity *I* of P2VP/OAPS nanocomposites as a function of the modulus of the scattering vector *q*. The intensity *I* for bulk P2VP/OAPS (main figure) and for thin films of P2VP/OAPS (inset).

peaks in intensity as a function of q for any OAPS fraction investigated here. This suggests that there is no observable periodic structure induced by the possible segregation of OAPS; if there were large OAPS aggregates present in the samples, broad peaks at low q would be expected to appear. The scattering pattern obtained by GISAXS also showed similar q-dependence of the intensity, which supports that even in the thin film geometry, there is no segregation of OAPS. Therefore, it was confirmed that the OAPS is not segregated but well dispersed in the P2VP matrix in all compositions and geometries.

The complex permittivity of these materials was then studied as a function of frequency and OAPS weight fraction (ϕ_{OAPS}) at a given temperature as shown in Figure 7a. The OAPS molecules form hydrogen bonds with the lone pair present on the 2VP monomers, which increases $T_{\rm g}$ due to the slowdown of segmental mobility. Interestingly and seemingly contrary to previous

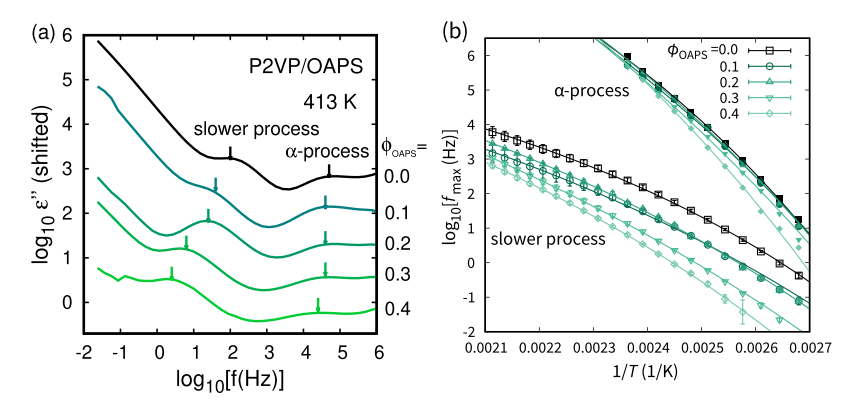


Figure 7. (a) Imaginary permittivity ε'' of P2VP/OAPS as a function of ϕ_{OAPS} . Curves are shifted vertically for clarity. The shift amounts are 3.0, 2.1, 1.3, 0.7, and 0 for $\phi_{OAPS} = 0$, 0.1, 0.2, 0.3, and 0.4, respectively. The slower process increases in strength and relaxation time with ϕ_{OAPS} , while the α -process remains largely unchanged. (b) Arrhenius plot of the slower process and the α -process, highlighting the large effect that ϕ_{OAPS} has on the slower process. A Kapton spacer with a thickness of 12.5 μ m was used. Thickness of P2VP/OAPS films ranges between 2.5 and 6 μ m. Fitting parameters are shown in Table S3.

reports, ^{14,15} the α -relaxation time was not substantially affected by the presence of OAPS fillers. Instead, the slower process relaxation time of P2VP increased with increased OAPS loading. Furthermore, both the α - and slower processes behave according to VFT across all ϕ_{OAPS} (Figure 7b). This may suggest that the OAPS interacts with the P2VP matrix similarly to the hypothesized impurities observed previously, where the OAPS motion is highly coupled to the slower process. Because OAPS itself shows two dielectric relaxation processes (Figure S6), it is expected that OAPS motion should be associated with the slow process at higher OAPS fractions larger than 40 to 100%. Further studies should identify the physical process by which the structural isotropization of a polymer segment is coupled to the transport of impurities/nanofillers in a matrix of the polymer.

The temperature dependence of the relaxation times of the slower process and the α -process can be described by the VFT law for all P(S-2VP) copolymers and P2VP/OAPS nanocomposites investigated here, as shown in Figures 4b and 7b. At lower temperatures, near glass transitions, the curves of both processes are approaching to each other so that both processes seem to be frozen at the same temperatures, except the low 2VP fraction of P(S-2VP) copolymers. This results suggest that there is a strong coupling between the slower process and the α process. The strength of the coupling is influenced by copolymerization with styrene monomers or loading of OAPS. As shown the above, the loading of OAPS seems to enhance the coupling of the slower process with the α -process, and as a result, the slower process can be used as a convenient monitor for measuring the effect of OAPS loading on the glassy dynamics in P2VP systems.

CONCLUSIONS

By introducing an air gap between the sample and the electrode in dielectric spectroscopy, we successfully observed an extra process (slower process) in addition to the α -process. The slower process occurs at much longer timescales than the α -process in P2VP and its random copolymers with styrene. In copolymers with high $f_{\rm 2VP}$, the slower process is well separated from the DC conductivity and is thus assigned to a conformational isotropization. In copolymers with lower $f_{\rm 2VP}$, the relaxation strength of the slower process dominates the α -process. This is reasonable if the slower process conformational isotropization is somehow coupled to charge carrying impurities, while the α -process is weak due to the very low polarity of styrene monomers.

To test the influences of additives within the polymer matrix, we collected data in a P2VP-OAPS nanocomposite, showing that the slower process was coupled to nanofiller polymer interactions. Intriguingly, the loading of OAPS influenced more on the slower process relaxation strength and relaxation time, rather than the α -relaxation time as expected. This could be explained by the OAPS behaving similarly to a charged impurity suggested by the neat copolymer data. Proper observation and understanding of the slower process are essential to understand the unconventional dynamics of nanocomposites containing P2VP. Ultimately, this report would inspire future experimental and computational research to understand this apparent relationship between the structural isotropization of polymer segments and mass transport of impurities/nanofillers through a polymer matrix, potentially with high-throughput dielectric spectroscopy. ³⁹

METHODS

Materials. For spacer thickness-dependent dielectric spectroscopy measurements, poly(2-vinylpyridine) $(M_n = 5 \text{ kDa}, M_w/M_n = 1.04, T_\sigma =$ 338.0 \pm 2.0 K) was purchased from Polymer Source (Dorval, QC, Canada). Tetrahydrofuran (THF) used for DRS measurements was purchased from FUJIFILM Wako Chemicals (Osaka, Japan). Hexanes, methanol, ethyl acetate, petroleum ether, fuming nitric acid, magnesium sulfate, ferric chloride, and Celite 545 were purchased from Fisher Scientific (Waltham, MA, USA). Azobisisobutyronitrile (AIBN) and tetrahydrofuran (THF) were purchased from Alfa Aesar (Haverhill, MA, USA). Styrene, 2-vinylpyridine, basic alumina, calcium hydride, and hydrazine hydrate were purchased from Acros Organics (Fair Lawn, NJ, USA). Octaphenyl silsesquioxane was purchased from Hybrid Plastics (Hattiesburg, MS, USA). Ethyl 2-(phenylcarbonothioylthio)-2phenylacetate and ethylamine solution (2 M in THF) were purchased from Sigma-Aldrich (St. Louis, MO, USA). AIBN was recrystallized in methanol. Styrene and 2-vinylpyridine were purified by passing through a column of basic alumina to remove inhibitor. Anisole was dried over calcium hydride. All other materials were used as received.

Octa(aminophenyl) Silsesquioxane Synthesis. OAPS was synthesized in-house from octaphenyl silsesquioxane (OPS) following literature procedures from Haibo et al. 40,41 Fifty grams of OPS was converted to octa(nitrophenyl) silsesquioxane (ONPS) via nitration reaction with nitric acid for 20 h at room temperature. This reaction produced an off-white powder at 81.0% yield. OPNS was converted to OAPS via a reduction step, with hydrazine hydrate as an in situ hydrogen source with ferric chloride catalyst, 5% Pd/C, and THF solvent reflux at 60 °C. The OAPS produced was a light brown powder at 78.2% yield for a total yield of 63.3%.

Poly(styrene-stat-2-vinylpyridine) Synthesis. Statistical copolymers of styrene and 2-vinyl pyridine were synthesized via reversible

addition fragmentation chain-transfer (RAFT) polymerization. 26 A total of 20 g of styrene and 2-vinylpyridine were added to a 250 mL round-bottom flask at different molar ratios with 15 mL of anisole. Ethyl 2-(phenylcarbonothioylthio)-2-phenylacetate was used as the RAFT chain transfer agent (CTA), with azobisisobutyronitrile (AIBN) as the initiator. Reagents were added at a 600:4:1 molar ratio of monomers to CTA to AIBN. The reaction was degassed with nitrogen for 30 min and then heated to 70 °C for 18 h, before quenching at 0 °C for 30 min and precipitating in hexanes two times. Polystyrene homopolymers were precipitated in methanol instead of hexanes. If applicable, RAFT endgroups were then cleaved by stirring the polymer in 0.5 M ethylamine solution in THF at room temperature for 30 min before precipitating two extra times in methanol. The pink powder was dried under reduced pressure at 80 °C for 24 h and characterized by NMR and gel permeation chromatography.

Nuclear Magnetic Resonance. NMR measurements were taken on a Bruker 500 500 MHz NMR instrument with cryoprobe attachments in solutions of acetone- d_6 at concentrations of 50 mg/mL.

Gel Permeation Chromatography. The molecular weight and dispersity of the P(S-2VP) copolymers synthesized were characterized via GPC in a mobile phase of dimethyl formamide (DMF) with 0.01 M lithium chloride salt at 50 °C relative to a polystyrene standard. The GPC instrument consisted of an Agilent Technologies 1260 Infinity, fitted with a Gel 5 μ m guard column, a PL Gel 5 μ m mix D 1° column, and a PL Gel 5 μ m Mix C 1° column. Samples were run at a flow rate of 1 mL/min using toluene as the flow rate marker.

X-ray Scattering. The X-ray scattering measurements were performed at BL40B2 of SPring-8, Nishiharima, Japan. Simultaneous small-angle X-ray scattering and wide-angle X-ray scattering (SAXS/WAXS) techniques were used for bulk measurements, with an X-ray wavelength of 0.09 nm. The X-ray cameras for SAXS and WAXS were Pilatus3S 2 M (Dectris) and a flat panel detector (Hamamatsu Photonics), respectively. The camera lengths were 89.0 mm for WAXS and 2287 mm for SAXS. For thin films measurements, grazing-incidence SAXS/WAXS (GISAXS/WAXS) techniques were used with an X-ray wavelength of 0.1 nm. Thin films for GISAXS/WAXS were prepared on Si substrate by the solution-casting method in the same way used for the preparation of samples for DRS measurements.

Dielectric Relaxation Spectroscopy. For DRS measurements, an impedance analyzer, an Alpha-A-high-performance frequency analyzer, was used together with a cooling unit, a Quatro cryosystem, from Novocontrol Technologies GmbH & Co. KG (Montabaur, Germany). Films for DRS measurements were prepared by drop-casting on the lower electrode from a THF solution of P2VP/OAPS with a concentration of 2 wt %, yielding a \sim 5 μ m coating. After annealing at RT for 24 h, the sample on the electrode was further annealed at 180 °C for 24 h under vacuum. To avoid any electrical short between upper and lower electrodes and to control the thickness of the air gap, a Kapton film with a small area with various thicknesses between 12.5 and 37.5 μ m was inserted between the upper and lower electrodes. DRS measurements were performed for the temperature range between 293 and 473 K and for the frequency range between 23 mHz and 1 MHz. The thickness of the polymer films was evaluated by performing capacitance measurements together with AFM measurements. The former gives us a relative but effective averaged thickness, while the latter does a local but absolute thickness. Combining the two methods enables us to evaluate the effective averaged thickness for all samples. Thickness evaluated in this way ranges between 4 and 8 μ m for P(S-2VP) copolymers and between 3 and 6 μ m for P2VP/OAPS nanocomposites.

Atomic Force Microscopy. For AFM measurements, a scanning probe microscopy SPM-9800 by Shimadzu Co. Ltd. in Japan was used together with dynamic mode cantilever NCHR by NanoWorld Co. Ltd. in Switzerland. Polymer films were prepared on glass substrates by the same procedure as for dielectric measurements. After making a step by scratching, the step height was measured as the absolute thickness of the polymer films. Using this absolute thickness, dielectric permittivity can be determined at a standard temperature and frequency.

ASSOCIATED CONTENT

Supporting Information

The Supporting Information is available free of charge at https://pubs.acs.org/doi/10.1021/acs.macromol.2c00789.

GPC and NMR of P(S-2VP) copolymers and OAPS, full DRS scans and fitting parameters of all copolymers, comparison of the timescale of the slower process to others from the literature, VFT fit parameters of copolymers and composites, DRS of OAPS, and a discussion of the possible influence of MWS polarization on the slower process (PDF)

AUTHOR INFORMATION

Corresponding Authors

Koji Fukao — Department of Physics, Ritsumeikan University, Kusatsu 525-8577, Japan; Email: kfukao@se.ritsumei.ac.jp Reika Katsumata — Department of Polymer Science and Engineering, University of Massachusetts Amherst, Amherst, Massachusetts 01003, United States; orcid.org/0000-0003-3119-9385; Email: rkatsumata@umass.edu

Authors

Walter W. Young — Department of Polymer Science and Engineering, University of Massachusetts Amherst, Amherst, Massachusetts 01003, United States; orcid.org/0000-0003-4358-9639

Hiromu Tabuchi — Department of Physics, Ritsumeikan University, Kusatsu 525-8577, Japan

Ryo Iguchi – Department of Physics, Ritsumeikan University, Kusatsu 525-8577, Japan

Takashi Konishi — Graduate School of Human and Environmental Studies, Kyoto University, Kyoto 606-8501, Japan; © orcid.org/0000-0003-1134-5445

Complete contact information is available at: https://pubs.acs.org/10.1021/acs.macromol.2c00789

Notes

The authors declare no competing financial interest.

ACKNOWLEDGMENTS

W.Y. acknowledges the financial support of a Department of Education GAANN Fellowship. K.F. acknowledges the financial support by a Grant-in-Aid for Scientific Research (B) (grant no. 19H01865) from the Japan Society for the Promotion of Science. R.K. acknowledges the support of NSF CAREER Award DMR #2046606 and UMass Amherst Startup Funding. The authors acknowledge the UMass Amherst Nuclear Magnetic Resonance Facility and the UMass Amherst Gel Permeation Chromatography Facility. The X-ray scattering measurements were performed at the BL40B2 of SPring-8 with the approval of the Japan Synchrotron Radiation Research Institute (JASRI) (proposal nos.2020A1348, 2021A1250, 2021B1420, and 2021B1422).

REFERENCES

- (1) Rubinstein, M.; Colby, R. H.Polymer Physics; 1st ed; Oxford University Press, 2003.
- (2) Kremer, F.; Schönhals, A.Broadband Dielectric Spectroscopy; Springer-Verlag: Berlin Heidelberg, 2003.
- (3) McCrum, N.; Read, B.; Williams, G. Anelastic and Dielectric Effects in Polymeric Solids; Dover Books on Engineering; Dover Publications, 1967.

- (4) Beiner, M. Relaxation in Poly(alkyl methacrylate)s: Crossover Region and Nanophase Separation. *Macromol. Rapid Commun.* **2001**, 22, 869–895.
- (5) Wind, M.; Graf, R.; Heuer, A.; Spiess, H. W. Structural Relaxation of Polymers at the Glass Transition: Conformational Memory in Poly(nalkylmethacrylates). *Phys. Rev. Lett.* **2003**, *91*, 155702.
- (6) Soles, C. L.; Burns, A. B.; Ito, K.; Chan, E.; Liu, J.; Yee, A. F.; Tyagi, M. S. Importance of Sub-Nanosecond Fluctuations on the Toughness of Polycarbonate Glasses. *Macromolecules* **2020**, *53*, 6672–6681.
- (7) Xiao, C.; Jho, J. Y.; Yee, A. F. Correlation between the Shear Yielding Behavior and Secondary Relaxations of Bisphenol A Polycarbonate and Related Copolymers. *Macromolecules* **1994**, 27, 2761–2768.
- (8) Jho, J. Y.; Yee, A. F. Secondary Relaxation Motion in Bisphenol A Polycarbonate. *Macromolecules* **1991**, 24, 1905–1913.
- (9) Li, X.; Yee, A. F. Design of Mechanically Robust High-Tg Polymers: Mechanical Properties of Glassy Poly(Ester Carbonate)s with Cyclohexylene Rings in the Backbone. *Macromolecules* **2004**, *37*, 7231–7239
- (10) Liu, J.; Yee, A. F. Enhancing Plastic Yielding in Polyestercarbonate Glasses by 1,4-Cyclohexylene Linkage Addition. *Macromolecules* **1998**, 31, 7865–7870.
- (11) Papadopoulos, P.; Peristeraki, D.; Floudas, G.; Koutalas, G.; Hadjichristidis, N. Origin of Glass Transition of Poly(2-Vinylpyridine). A Temperature- and Pressure-Dependent Dielectric Spectroscopy Study. *Macromolecules* **2004**, *37*, 8116–8122.
- (12) Bocharova, V.; Genix, A.-C.; Carrillo, J.-M. Y.; Kumar, R.; Carroll, B.; Erwin, A.; Voylov, D.; Kisliuk, A.; Wang, Y.; Sumpter, B. G.; Sokolov, A. P. Addition of Short Polymer Chains Mechanically Reinforces Glassy Poly(2-Vinylpyridine)-Silica Nanoparticle Nanocomposites. *ACS Appl. Nano Mater.* **2020**, *3*, 3427–3438.
- (13) Voylov, D. N.; Holt, A. P.; Doughty, B.; Bocharova, V.; Meyer, H. M., III; Cheng, S.; Martin, H.; Dadmun, M.; Kisliuk, A.; Sokolov, A. P. Unraveling the Molecular Weight Dependence of Interfacial Interactions in Poly(2-Vinylpyridine)/Silica Nanocomposites. *ACS Macro Lett.* **2017**, *6*, 68–72.
- (14) Cheng, S.; Xie, S.-J.; Carrillo, J.-M. Y.; Carroll, B.; Martin, H.; Cao, P.-F.; Dadmun, M. D.; Sumpter, B. G.; Novikov, V. N.; Schweizer, K. S.; Sokolov, A. P. Big Effect of Small Nanoparticles: A Shift in Paradigm for Polymer Nanocomposites. *ACS Nano* **2017**, *11*, 752–759.
- (15) Bailey, E. J.; Griffin, P. J.; Composto, R. J.; Winey, K. I. Multiscale Dynamics of Small, Attractive Nanoparticles and Entangled Polymers in Polymer Nanocomposites. *Macromolecules* **2019**, *52*, 2181–2188.
- (16) Bailey, E. J.; Griffin, P. J.; Tyagi, M.; Winey, K. I. Segmental Diffusion in Attractive Polymer Nanocomposites: A Quasi-Elastic Neutron Scattering Study. *Macromolecules* **2019**, *52*, 669–678.
- (17) Popov, I.; Carroll, B.; Bocharova, V.; Genix, A.-C.; Cheng, S.; Khamzin, A.; Kisliuk, A.; Sokolov, A. P. Strong Reduction in Amplitude of the Interfacial Segmental Dynamics in Polymer Nanocomposites. *Macromolecules* **2020**, *53*, 4126–4135.
- (18) Cheng, S.; Sokolov, A. P. Correlation between the Temperature Evolution of the Interfacial Region and the Growing Dynamic Cooperativity Length Scale. *J. Chem. Phys.* **2020**, *152*, No. 094904.
- (19) Cheng, S.; Holt, A. P.; Wang, H.; Fan, F.; Bocharova, V.; Martin, H.; Etampawala, T.; White, B. T.; Saito, T.; Kang, N.-G.; Dadmun, M. D.; Mays, J. W.; Sokolov, A. P. Unexpected Molecular Weight Effect in Polymer Nanocomposites. *Phys. Rev. Lett.* **2016**, *116*, No. 038302.
- (20) Lin, Y.; Liu, L.; Xu, G.; Zhang, D.; Guan, A.; Wu, G. Interfacial Interactions and Segmental Dynamics of Poly(Vinyl Acetate)/Silica Nanocomposites. *J. Phys. Chem. C* **2015**, *119*, 12956–12966.
- (21) Holt, A. P.; Griffin, P. J.; Bocharova, V.; Agapov, A. L.; Imel, A. E.; Dadmun, M. D.; Sangoro, J. R.; Sokolov, A. P. Dynamics at the Polymer/Nanoparticle Interface in Poly(2-Vinylpyridine)/Silica Nanocomposites. *Macromolecules* **2014**, *47*, 1837–1843.
- (22) Kumar, S.; Benicewicz, B.; Vaia, R.; Winey, K. 50th Anniversary Perspective: Are Polymer Nanocomposites Practical for Applications? *Macromolecules* **2017**, *50*, 714–731.

- (23) Serghei, A.; Kremer, F. Broadband Dielectric Spectroscopy on Ultrathin Organic Layers Having One Free (Upper) Interface. *Rev. Sci. Instrum.* **2006**, *77*, 116108.
- (24) Serghei, A.; Huth, H.; Schick, C.; Kremer, F. Glassy Dynamics in Thin Polymer Layers Having a Free Upper Interface. *Macromolecules* **2008**, *41*, 3636–3639.
- (25) Sanno, N.; Murakami, I.; Yamamura, H. Dielectric β -Relaxation in Poly(2- vinylpyridine). *Polymer J.* **1976**, *3*, 231–238.
- (26) Young, W. W.; Saez, J. P.; Katsumata, R. Rationalizing the Composition Dependence of Glass Transition Temperatures in Amorphous Polymer/POSS Composites. *ACS Macro Lett.* **2021**, *10*, 1404–01409.
- (27) Yano, O.; Wada, Y. Dynamic mechanical and dielectric relaxations of polystyrene below the glass temperature. *J. Polym. Sci., Part A-2* **1971**, *9*, 669–686.
- (28) Fukao, K.; Miyamoto, Y. Dielectric relaxation of isotactic polystyrene above the glass transition temperature. *Polymer* **1993**, *34*, 238–246.
- (29) Havriliak, S.; Negami, S. A complex plane representation of dielectric and mechanical relaxation processes in some polymers. *Polymer* **1967**, *8*, 161–210.
- (30) Fulcher, G. S. Analysis of Recent Measurements of the Viscosity of Glasses. *J. Am. Ceram. Soc.* **1925**, *8*, 339–355.
- (31) Fulcher, G. S. Analysis of Recent Measurements of the Viscosity of Glasses.—II¹. *J. Am. Ceram. Soc.* **1925**, *8*, 789—794.
- (32) Vogel, H. Das Temperatur-Abhängigkeitsgesetz der Viskosität von Flüssigkeiten. *Phys. Z.* **1921**, 22, 645–646.
- (33) Tammann, G.; Hesse, W. Die Abhängigkeit der Viscosität von der Temperatur bie unterkühlten Flüssigkeiten. *Z. Anorg. Allg. Chem.* **1926**, 156, 245–257.
- (34) Song, Z.; Rodriguez-Tinoco, C.; Mathew, A.; Napolitano, S. Fast equilibration mechanisms in disordered materials mediated by slow liquid dynamics. *Sci. Adv.* **2022**, *8*, eabm7154.
- (35) Lupaşcu, V.; Picken, S. J.; Wübbenhorst, M. Dynamics of T2G2 Helices in Atactic and Syndiotactic Polystyrene: New Evidence from Dielectric Spectroscopy and FTIR. *Macromolecules* **2006**, 39, 5152–5158.
- (36) Müller-Buschbaum, P. Grazing incidence small-angle X-ray scattering: an advanced scattering technique for the investigation of nanostructured polymer films. *Anal. Bioanal. Chem.* **2003**, 376, 3–10.
- (37) Roth, S. V.; Burghammer, M.; Riekel, C.; Müller-Buschbaum, P.; Diethert, A.; Panagiotou, P.; Walter, H. Self-assembled gradient nanoparticle-polymer multilayers investigated by an advanced characterization method: microbeam grazing incidence x-ray scattering. *Appl. Phys. Lett.* **2003**, *82*, 1935–1937.
- (38) Lee, B.; Park, I.; Yoon, J.; Park, S.; Kim, J.; Kim, K.-W.; Chang, T.; Ree, M. Structural Analysis of Block Copolymer Thin Films with Grazing Incidence Small-Angle X-ray Scattering. *Macromolecules* **2005**, 38, 4311–4323.
- (39) Zhang, X.; Zhao, J.; Ye, C.; Lai, T.-Y.; Snyder, C. R.; Karim, A.; Cavicchi, K. A.; Simmons, D. S. Dynamical Correlations for Statistical Copolymers from High-Throughput Broad-Band Dielectric Spectroscopy. *ACS Comb. Sci.* **2019**, *21*, 276–299.
- (40) Haibo, F.; Rongjie, Y.; Dinghua, L. Synthesis Improvement and Characterization of Polyhedral Oligomeric Octa(aminophenyl)-silsesquioxane. *Acta Chim. Sin.* **2012**, *70*, 429.
- (41) Tamaki, R.; Tanaka, Y.; Asuncion, M. Z.; Choi, J.; Laine, R. M. Octa(aminophenyl)silsesquioxane as a Nanoconstruction Site. *J. Am. Chem. Soc.* **2001**, *123*, 12416–12417.